Processability and Mechanical Properties of Ternary Composites PP/EPDM/GF

SILVIA E. BARBOSA* *and* NUMA J. CAPIATI

PLAPIQUI (UNS-CONICET)
C.C. 717- (8000) Bahía Blanca, Argentina

and

JOSÉ M. KENNY

Materials Engineering Center
University of Perugia
Pentima Bassa 21, (05100) Terni, Italy

The enhancement of the mechanical properties of neat PP is achieved by the addition of glass fibers and EPDM rubber. The Young's modulus and notched Charpy impact strength of the composites obtained are improved with respect to the original polymer, leading to a new composite material with a very good balance of toughness and rigidity properties. The tensile behavior of these multiphase systems is successfully compared with theoretical predictions using the Halpin-Tsai/Nielsen theory for uniaxially short fiber composites, which considers the matrix as a blend with spherical particles and can predict the tensile modulus considering an average fiber orientation angle. An accurate morphological study performed by scanning electron microscopy (SEM) shows a very good dispersion of the rubbery phase into the neat matrix. No special affinity between the rubber and the fibers is reported. The good dispersion and the small particle diameter indicate the good processability of the ternary systems studied.

INTRODUCTION

The modification of polypropylene (PP) by rubber blending or filler addition is a well-known route to improve its mechanical properties. The incorporation of short fibers enhances its tensile properties (1–6). The use of this type of fillers in thermoplastics generates new materials that combine the versatility of PP manufacturing with the mechanical properties of the fibers (7, 8). These materials are very attractive because they are economic and recyclable.

However, short fiber reinforced PP does not show a very significant increase of the impact behavior with respect to neat polypropylene. Several attempts have been reported to enhance the toughness of polypropylene by blending with different elastomers generating incompatible binary blends (9–13). These blends have very good impact behavior but poor rigidity. On the other hand, the development of ternary blends as PP/elastomer/PE allowed the production of materials with higher impact strength and tensile properties than PP/elastomer binary blends (14, 15), but with lower tensile properties than neat PP.

The use of fillers and fibers in PP matrix materials has been widely adopted with the aim of generating a material with a good balance of toughness and rigidity properties. The use of ternary compounds PP/elastomer/mineral fillers (talc, calcium carbonate, etc.) (16–21) has allowed the achievement of materials with an approximate good balance of mechanical properties; but, in general, it has been demonstrated that the elastomer encapsulates the filler, improving impact strength but offering only a poor rigidity improvement.

Gupta *et al.* (22) reported the rheological and morphological effects of the inclusion of short glass fibers in PP/EPDM blends. They found that glass fibers do not affect the melt viscosity very much. They also concluded that EPDM particles remain on the fiber surface. This conclusion is not evident from the microphotographs shown by the authors because the rubbery phase was not extracted, and thus, it is indistinguishable in the observation of fracture surfaces by SEM.

*To whom correspondence should be addressed.

The interaction between the PP matrix, the rubbery phase, and the fillers is a very complex question, the chief factor in developing composites with optimum properties. In this work, EPDM was added to short glass fiber reinforced polypropylene in order to obtain a material with an improved balance of impact resistance and tensile modulus. Then, the preparation of composites with different content of fibers and elastomer and their processing by injection molding is reported. Moreover, the study includes the determination of the mechanical and impact properties and their analysis and comparison with theoretical predictions and accurate morphological studies.

EXPERIMENTAL

Materials: The material used in this research was glass fiber reinforced polypropylene modified with elastomers. Cuyolén H1NF301 kindly supplied by Petroquímica Cuyo (Argentina) in pellets with 30 % wt. of glass fibers was used as short fiber reinforced polypropylene. This SFRPP was based on PP injection grade (Mw = 250,000—Mn = 54,000), the average fiber length before processing was 2.5 mm and the fiber diameter was 13 μm. Ethylene-propylene-diene terpolymers (EPDM), with Mooney viscosity 38 and E/P ratio 66/34 was used as elastomer. The viscosity ratio between the elastomer and PP at the mixing conditions is 2.3.

Compounding: Different proportions of the SFRPP and the elastomer were mixed mechanically to prepare compounds with different fiber weight concentrations. These compounds were blended by melt extrusion in a Goettfert counter-rotating twin screw extruder (D = 35 mm, L/D = 20) with a 2 mm cylindrical die at 15 rpm. Four different elastomer/fiber weight fractions, named C0, C1, C10, C20, were prepared and tested. The respective concentrations are shown in *Table 1*. Barrel temperature profile for extruding was 120°C-190°C-200°C-210°C-220°C from the hopper to the die and was kept constant during extrusion.

Molding: The new material was pelletized and molded in a Fluidmec 60t injection-molding machine with the following injection parameters:

Screw speed: 100 rpm

Back pressure: 10^6 Pa

Barrel temperature profile (°C): 180–190–200–200

Die temperature (°C): 220

Injection Pressure: 6.6×10^6 Pa

Hold pressure profile: (% of P max): 60-60-50-40-30-30-30-25-20 (P_{max}: 1.1 10^7 Pa)

Injection speed profile: (% max inj. speed) 40-50-60-50-45-40-30-20-20 (Is_{max}: 15 cm/s)

Injection time: 1 s

Hold time: 4 s

The value of the back pressure was defined after several trials. This value is the optimum, which balances the very good dispersion of the elastomer with small particles but higher attrition on the fibers, obtained with high back pressure and the improvement of the final fiber length, accompanied with higher elastomeric particles, obtained when no back pressure is applied. The mold used has two cavities to produce tensile and Charpy impact test coupons with nominal dimensions according to ASTM D638 and ASTM D256. In both cavities, the material was injected from one of the ends as shown in *Fig. 1*.

Testing: Tensile modulus was measured with a Lloyd automated materials testing system with transversal velocity of 5 mm/min. The test was carried out following ASTM D638M. The impact strength was measured on a Ceast 2000 Instrumented Impact Pendulum with 7.5 J as maximum energy, 3.46 m/s as maximum speed and hammer weight of 1.254 Kg. The Charpy notched test was carried out following ASTM D256.

Characterization: The analysis of the composite morphology was performed by scanning electronic microscopy (SEM) of the samples after extrusion and after testing. In the first case, cross sections were obtained by fracturing extruded filaments in liquid nitrogen, and in the second case, the section analyzed was the one remaining after fracture in tensile and impact tests. In both cases, the surface was treated with toluene into an ultrasonic chamber to extract the elastomeric phase. Samples were then dried and observed by SEM. Particle diameter (D_p) was determined by image analysis of SEM microphotographs and the average values obtained after each process are listed in *Table 1*.

Glass fiber final length distributions were determined by image analysis of more than 2000 fragments after ashing samples in a convection oven at 450°C for 5 hours. This analysis was performed on the original commercial compound and on all the formulations with different fiber concentrations, after

Table 1. Weight Composition and Characteristic Dimensions of the System Investigated After Extrusion and After Injection Molding.

Composite	Weight Fractions (%)			After Extrusion		After Injection Molding	
	PP	GF	EPDM	av. L (mm)	av. D_p (μm)	av. L (mm)	av. D_p (μm)
C0	100	0	0	—	—	—	—
C1	70	30	0	2.5	—	1.9	—
C10	63	27	10	1.7	0.8	1.5	0.95
C20	56	24	20	1.6	0.9	1.3	1.05

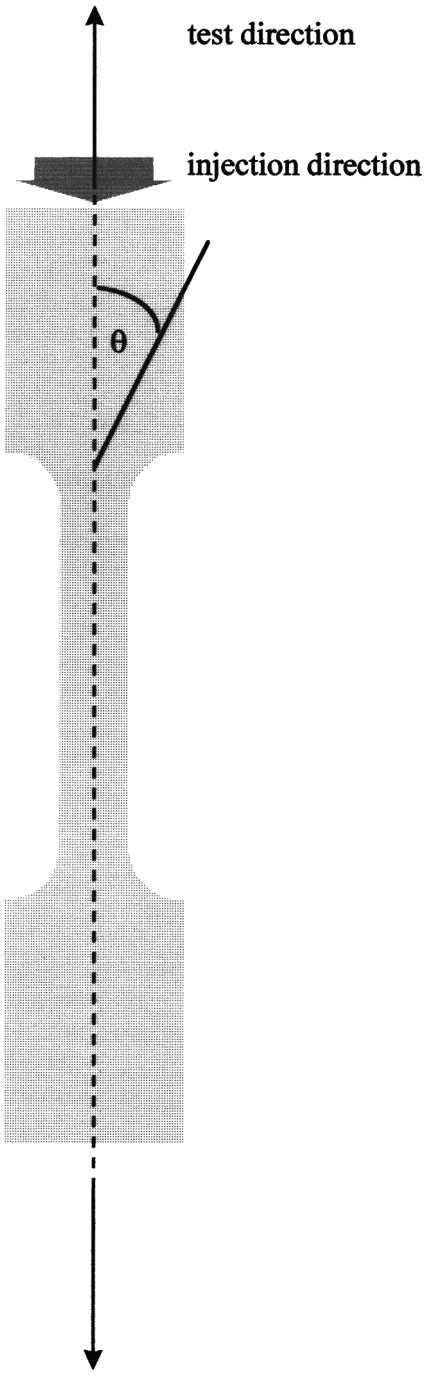

Fig. 1. Injection molding and tensile test directions.

extrusion and after injection molding, in order to compare the effect of the different processing operations on the fiber-matrix attrition. The average fiber length (L_f) measured values are reported in *Table 1*.

RESULTS AND DISCUSSION

Mechanical Properties

Tensile stress-strain curves for all of the composites analyzed and neat PP are reported in *Fig. 2*. The original binary composite C1, with 30 wt%. SFRPP showed, as expected, a brittle behavior with the highest elastic modulus. All the binary (PP/GF) composite samples tested showed a little knee around 0.5% of strain. This change in the curvature could be attributed to inhomogeneities in the fiber orientation distribution, which could induce the fracture of different layers with different fiber orientation distribution. In the fracture mechanism of SFRPP, the fiber ends behave as stress concentrators; this stress concentration within the damage zone gives rise to crazing in the polypropylene matrix, generating debonding along the fiber surface. The final crack path emerges by connection of the different craze planes because of fiber debonding, pullout and fracture events with concomitant matrix deformation. This path is strongly affected by fiber orientation distribution. When the fibers are oriented parallel to the craze direction, the path is encouraged (23). If it is considered that the tensile specimens were injected from one of the extremes and that the tensile test is performed in the same injection direction, then it can be concluded that most fibers are oriented on this axis (0° angle). However, because of the flow patterns during injection, different layers with different fiber orientation distributions can be obtained in the injected samples (24). Typically, on the surface region, fibers are more oriented on the flux direction while in the center, the fiber orientation is more random, as shown in *Fig. 1*. Then, the different layers contribute and resist in different forms during tensile testing. When the tensile test progresses, the load increases and the fibers oriented with larger angles with respect to the tensile direction yield and the resistance to the stress is mainly supported by the fibers oriented in the sense of the tensile stress until failure occurs. A similar but more marked behavior was found by Watanabe *et al.* (25) in sheet molding compound composites containing randomly oriented chopped fibers in a termosetting matrix. Obviously, the extreme of this behavior is determined by long fiber cross ply laminates (2). The "layered" structure was tested and observed by SEM micrographs shown below.

In the case of binary blends (PP/EPDM), elastomer particles act as stress concentrators in the surrounding matrix area generating crazes from the equatorial zones of rubber particles that propagates perpendicularly to the direction of the load. Crazes may grow favoring cracks and long craze bands. After their formation, cracks are stopped by weak rubber particles that delay the propagation of cracks and the ultimate fracture. On the other hand, ternary composites C10 and C20 show a particular tensile behavior. The elastic modulus and ultimate strength decrease when the rubber content increases but the ultimate strain increases. This complex behavior can be explained as a combination of the two fracture mechanisms described above. In ternary composites there are two types of stress concentrators, rubber particles and fiber ends. Evidently, the density of crazes increases and the superposition of fiber and rubber effects determine

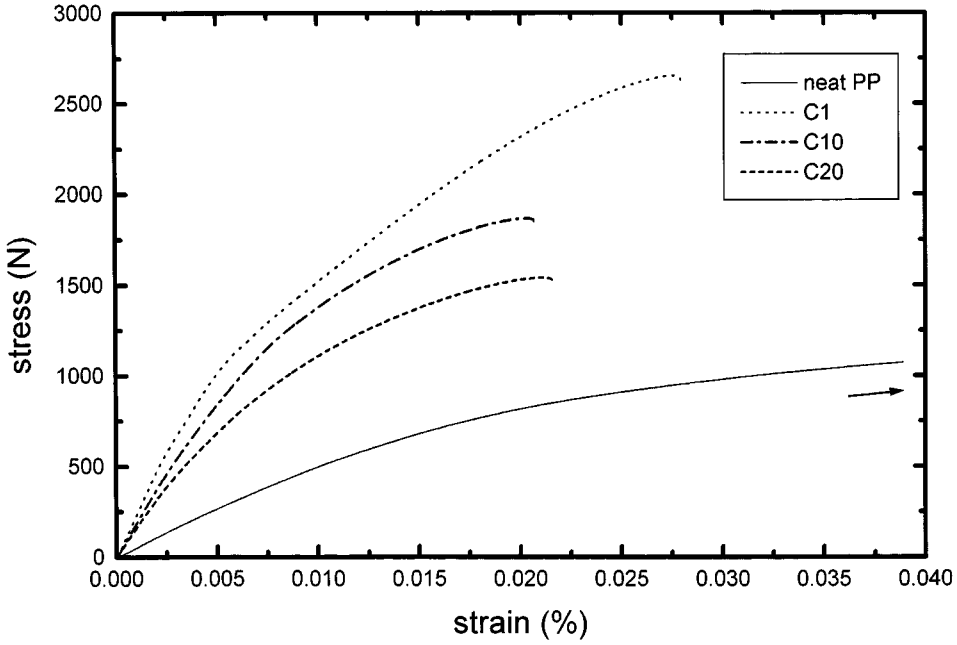

Fig. 2. Stress-strain curves for neat PP (continuous line), C1 (dotted line), C10 (dotted- dashed line) and C20 (dashed line).

that, when the quantity of particles is highest and the fiber content lower (24%) as in composite C20, the crack propagation initiated in fiber ends, is more attenuated. Then, the material is more resistant and the ultimate strain is higher than in the case of composite C10 where the content of rubber and the total quantity of particles is lower (approximately half of C20) and the content of fibers (27%) is higher.

The knee is not evident in C10 and C20 probably because the stress-strain behavior of the matrix (binary blend) masks the effect of fiber orientation distributions as explained above. However, also in this case the "layered" structure was observed by SEM microphotography as reported below. No differences were observed in the average dimension of the elastomer particles measured in the different fiber orientation layers. However, a marked difference in particle forms was observed in the central layer where most particles were oval with the major axis oriented in the flux direction. In the other regions of the samples, the particles were circular.

Elastic modulus data were compared with theoretical predictions for short fiber composites. In uniaxial composites, the Young's Modulus (E_θ) at any angle with respect to the fiber direction can be represented by the following equation (3):

$$\frac{1}{E_\theta} = \frac{\cos^4\theta}{E_L} + \frac{\sin^4\theta}{E_T} + \left(\frac{1}{G_{LT}} - \frac{2\nu_{LT}}{E_L}\right)\sin^2\theta\cos^2\theta \quad (1)$$

Where E_L, E_T and G_{LT} are the longitudinal, transversal and longitudinal-transverse shear moduli respectively, θ is the angle between the fibers and the direction of the tensile load applied. In general all moduli can be calculated by the Halpin-Tsai equations modified by Nielsen (3) as:

$$M = M_m\left(\frac{1 + AB\phi_f}{1 - B\psi\phi_f}\right) \quad (2)$$

where M is the modulus of the composite, M_M is the corespondent matrix modulus, ϕ_f is the fiber volume fraction and B and ψ are parameters given by the following expressions:

$$B = \frac{E_m/E_f - 1}{E_m/E_f + A} \qquad \psi \doteq 1 + \frac{1 - \phi_M}{\phi_M^2}\,\phi_f \quad (3)$$

E_m and E_f are the moduli of the matrix and fibers respectively and (L/D) is the aspect ratio of the fibers. The factor ψ takes into account the maximum packing fraction ϕ_M of the fibers. This value can be calculated theoretically for different spatial arrays of fibers. For cubic packing of fibers $\phi_M = 0.785$ while for hexagonal packing is 0.907. The constant A is different for the calculus of each modulus and takes into account filler geometry and orientation, and the nature of the matrix. For uniaxial fiber orientation, A = 2(L/D) for the calculus of E_L, A = 0.5 for E_T and A = 1 for G_{LT}. ν_{LT} is the Poisson's ratio of the composite for a tensile load applied parallel to the fibers and can be calculated as:

$$\nu_{LT} = \nu_f\phi_f + \nu_m\phi_m \quad (4)$$

where ν_m, ν_f, ϕ_m and ϕ_f are the Poisson's ratio and volume fractions of the matrix and fibers respectively.

The matrix for C1 was neat PP, and then E_m was the E_{PP} measured. However, in C10 and C20 the matrix of the composite is a binary blend with different elastomer content. In these cases, E_m was calculated accordingly to *Eqs 2* and *3* assuming spherical fillers (elastomeric particles) with an average diameter. The

Table 2. Parameters Used in Theoretical Computations.

Property	Polypropylene	Glass Fibers	EPDM
E (Mpa)	1198	72400	10
Poisson ratio	0.33	0.2	0.48
G_{LT} (Mpa)	503	30167	—
ρ(g/cm^3)	0.9	2.56	0.86
Max. packing fraction ϕ_M.	—	0.785*	0.79

*Value for cubic packing.

actual volume fraction of the elastomer (ϕ'_e) and the factor A for the blend were calculated as (3):

$$\phi'_e = \frac{\phi_e}{1 - \phi_f} \qquad A = \frac{8 - 10\nu_m}{7 - 5\nu_m} \tag{5}$$

where ϕ_e and ϕ_m are the volume fraction of the elastomer and of the fibers in the composite respectively and ν_m is the Poisson's ratio of the matrix (PP in this case). The material parameters used in the model are listed in *Table 2* and the theoretical predictions are shown in *Fig. 3*, where the computed composite Young's modulus is represented as a function of the fiber content and compared with experimental values. The straight line corresponds to the theoretical predictions with all the fibers in the load direction (uniaxial 0° angle). The dash line shows the theoretical predictions considering all the fibers perpendicular to the load (uniaxial 90° angle). Circles show the measured Young's modulus and these values are in very good agreement with those obtained by considering all fibers uniaxially oriented with an angle of 11.5° (dotted line). As described above, most of the fibers are oriented in the direction of the flux, but in the center of the sample there is a layer with a different fiber orientation; then, the composite can be modeled as uniaxial with a resulting average fiber orientation angle of 11.5°.

Figure 4 shows Charpy notched impact strength results plotted as a function of the Young's modulus of the same material for the different materials studied. Taking the impact strength of the neat PP as a reference point, the addition of the fibers duplicates the impact resistance, and, when 10% of elastomer is added, the impact strength triplicates. Moreover, when 20% of EPDM was added, the impact strength was increased six times more than that one of neat PP. On the other hand, the addiction of 30 wt% of fibers increases the Young's modulus of PP six times. When the elastomer was introduce to the composite C1, the Young modulus decreases, but in all of the cases the modulus of near PP was improved. It can be observed that C10 and C20 gave a very good balance of toughness and stiffness properties compared with neat PP or the binary composite (SFRPP).

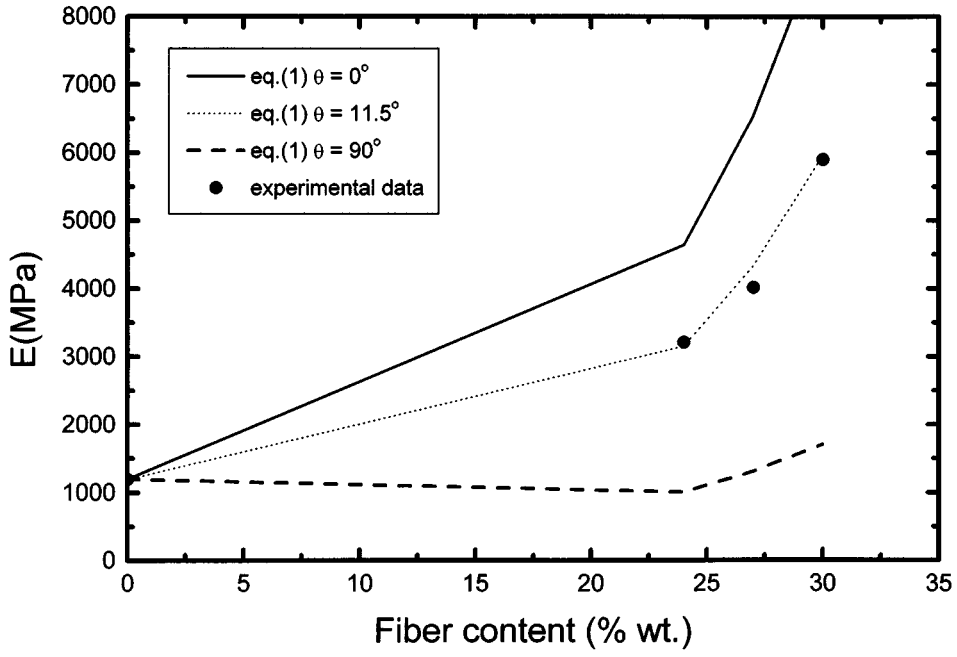

Fig. 3. Theoretical and experimental curves for Young modulus vs. fiber content for the different composites analyzed and for different average fiber angles.

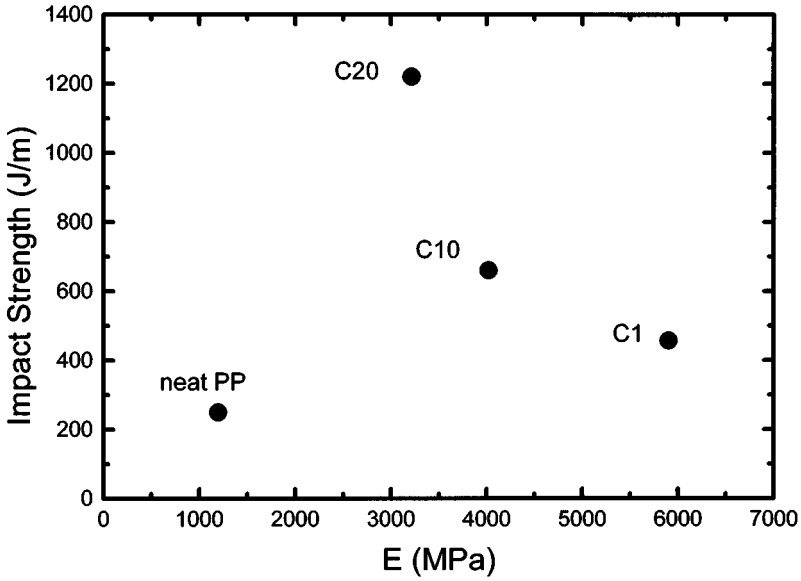

Fig. 4. Impact strength vs. Young's modulus for neat PP and the different composites studied.

Final fiber length is a very important factor to determine the grade of reinforcement in short fiber composites. There are several studies about this fact in different forms of processing SFRPP (26, 27). In this study, fiber damage occurs in two processing operations, compounding by twin screw extrusion and molding by injection. The measurements of the fiber's damage after each operations are listed in *Table 1*. From these values it may be concluded that the major damage occurs in the compounding operation; however, if the final length obtained is greater that the critical length (2–26), then the fiber reinforcement was effective. Critical fiber length is the minimum value of fiber length required for the fiber stress to be equal to the fiber ultimate strength at this midlength.

Final elastomer particle dimensions after each operation are listed in *Table 1*. These average values shown that the very good dispersion obtained after compounding was maintained after molding. Note that an study of the effect of the back pressure in this matter was done and applied as explained above.

Analysis of Composite Morphology

The analysis of the morphology of both composite formulations with rubber addition (C10 and C20) demonstrates a very good dispersion of the elastomer in the PP. Moreover, this dispersion is not strongly affected by the successive processing operations. The microstructure of both compounds is shown in *Fig. 5* (after extrusion) and in *Fig. 6* (after injection molding). The lower rubber content of the C10 composite is confirmed in both *Figures*. Moreover, the average particle diameter of the C10 sample is smaller than that of the C20 and this value increases slightly after injection molding as shown in *Table 1*. This is an interesting result as there was not a strong particle coalescence and final properties were clearly improved as shown above. There were no particular agglomerates of elastomer around the fibers in any of the conditions tested. *Figure 7* shows a microphotograph of a fractured surface of the short fiber reinforced polypropylene with 20% of glass fibers. The difference between the matrix surface is evident. In this case, the matrix is a continuos phase of neat PP.

Figure 8 shows a microphotograph of one fiber in the composite with 20% of elastomer. The matrix remaining around the pulled fibers is an indication of the good fiber-matrix adhesion. This microphotograph, also shows that the elastomer dispersion is very good and that there are no special agglomerates of rubber particles near the fibers. *Figure 9* shows a microphotograph obtained at a very high magnification (15,000×), where the fiber-matrix interface can be observed confirming the good adhesion shown before.

Figure 10 shows a fiber hole after the fracture. Small particles attached to the fibers can be observed in the hole. It can also be observed that the particles are uniformly distributed around the surface with no preferential locations. It is then possible to emphasize that in the materials analyzed the fibers are not encapsulated by the rubber particles as reported by other authors. In fact, it has been reported that the rubber (16–22) typically encapsulates fillers. This probably happens because all the particles have similar dimensions.

CONCLUSIONS

The mechanical properties of neat PP have been improved by incorporation of glass fibers and EPDM rubber. Young's modulus and notched Charpy impact strength are clearly higher in the ternary systems that

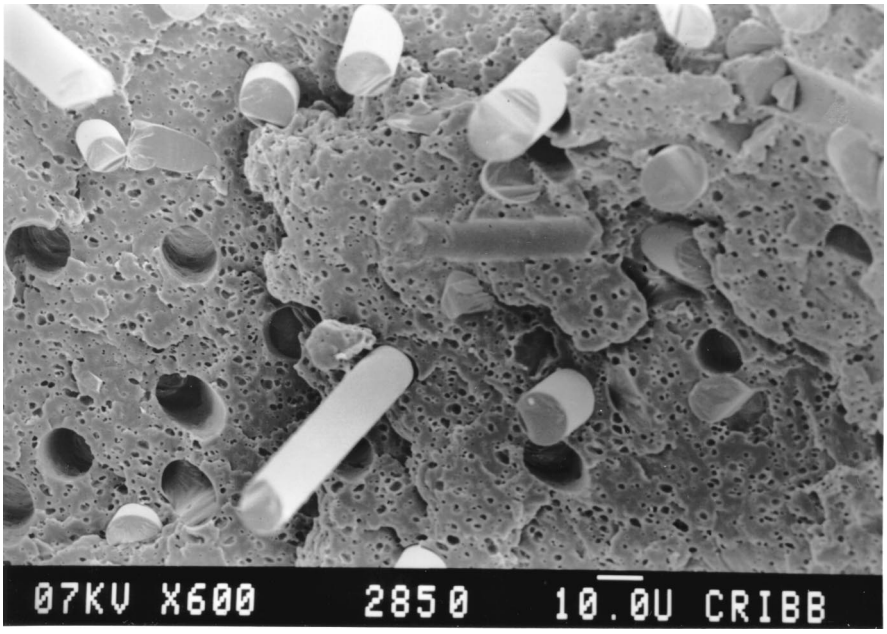

(a)

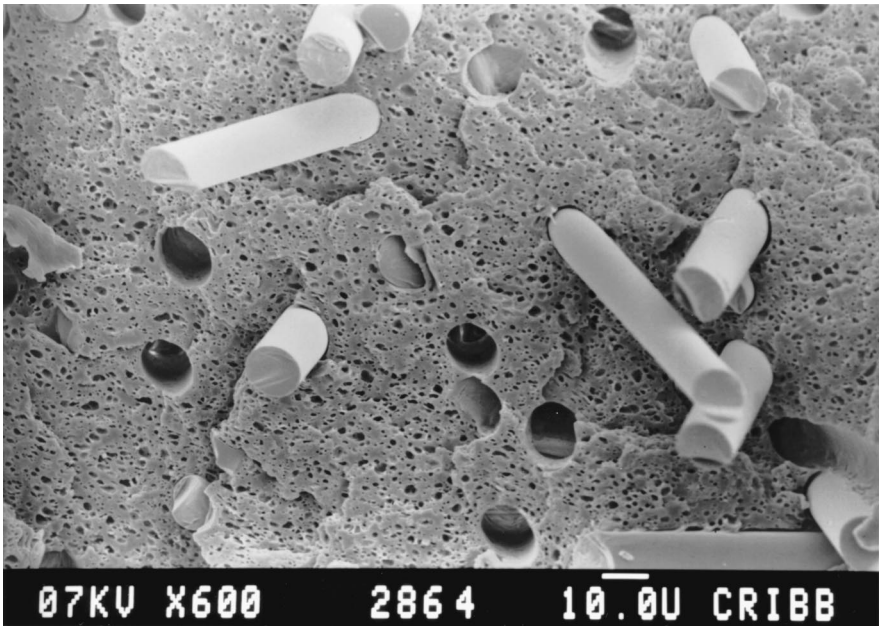

(b)

Fig. 5. SEM microphotographs of PP/EPDM/GF composites after compounding (600×): a) C10: 10% EPDM; b) C20: 20% EPDM.

combine the energy absorption capability of the rubber and the higher modulus of the glass fibers.

The tensile behavior of these multiphase systems can be described by the Halpin-Tsai/Nielsen theory by assuming an average fiber orientation angle of 11.5°.

An excellent dispersion of small rubber particles in the PP matrix has been obtained in the processed materials. Moreover, SEM analysis has shown a very good matrix-fiber interaction with no special affinity of the rubber with the fiber. No encapsulation effects of the elastomeric phase on the fibers have been detected.

The reported results demonstrate the excellent combination of mechanical properties and processability of the ternary PP/EPDM/GF studied.

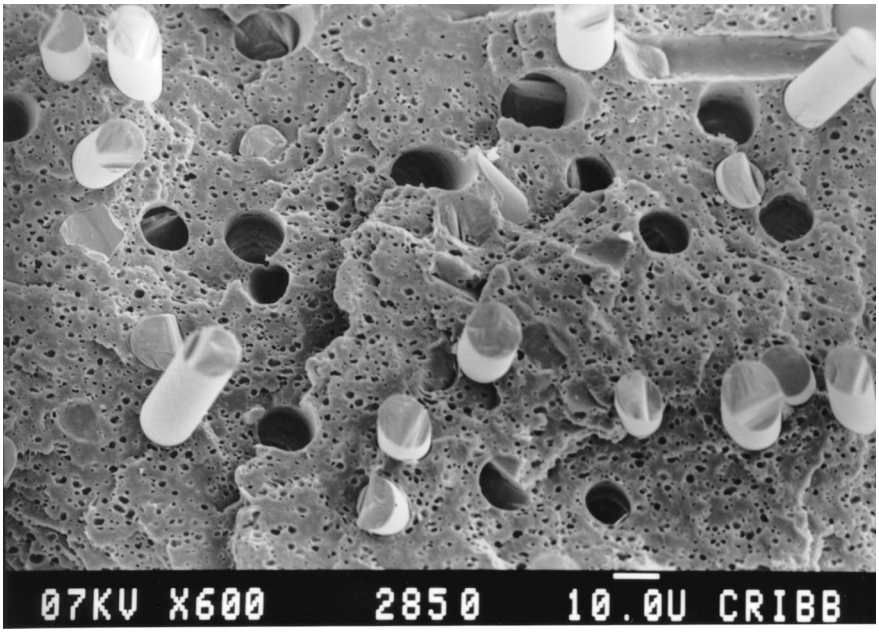

(a)

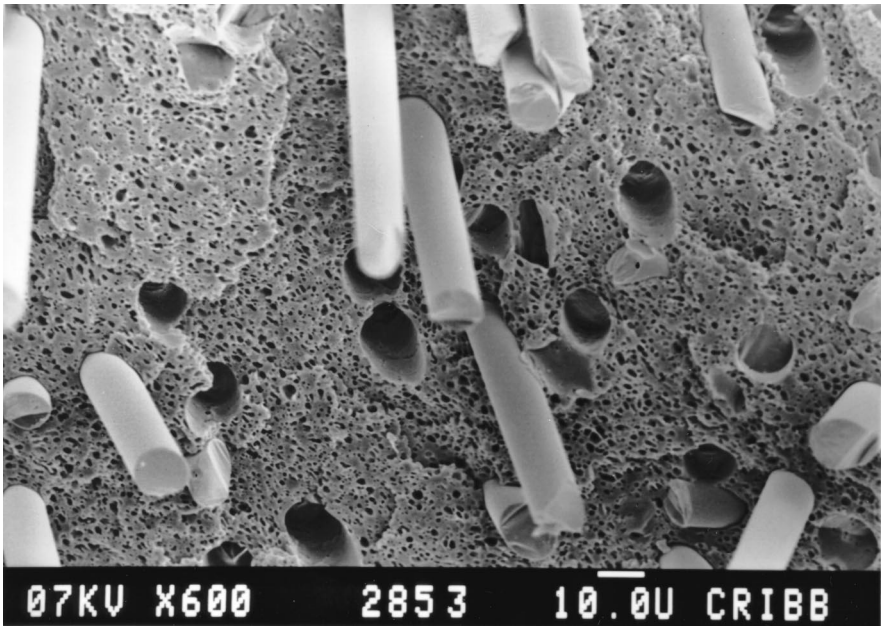

(b)

Fig. 6. SEM microphotograph of PP/EPDM/GF composites after injection molding (600×) a) C10: 10% EPDM. b) C20: 20% EPDM.

ACKNOWLEDGMENTS

This study was financed with a grant from the Argentine National Research Council (CONICET). The authors are thankful to Mr. Pablo Alberio for the specimen preparation and to Dr. Alberto Anunziata for the collaboration in impact measurements.

REFERENCES

1. C-E Wilen, M. Falden-Nylund, and J. Näsman, *J. Appl. Polym. Sci.*, **50**, 1541 (1993).
2. P. K. Mallik, *Fiber-Reinforced Composites: Materials, Manufacturing and Design*, Marcel Dekker, Inc. (1988).
3. L. Nielsen and R. Landel, *Mechanical Properties of Polymers and Composites*, Marcel Dekker, Inc. (1994).

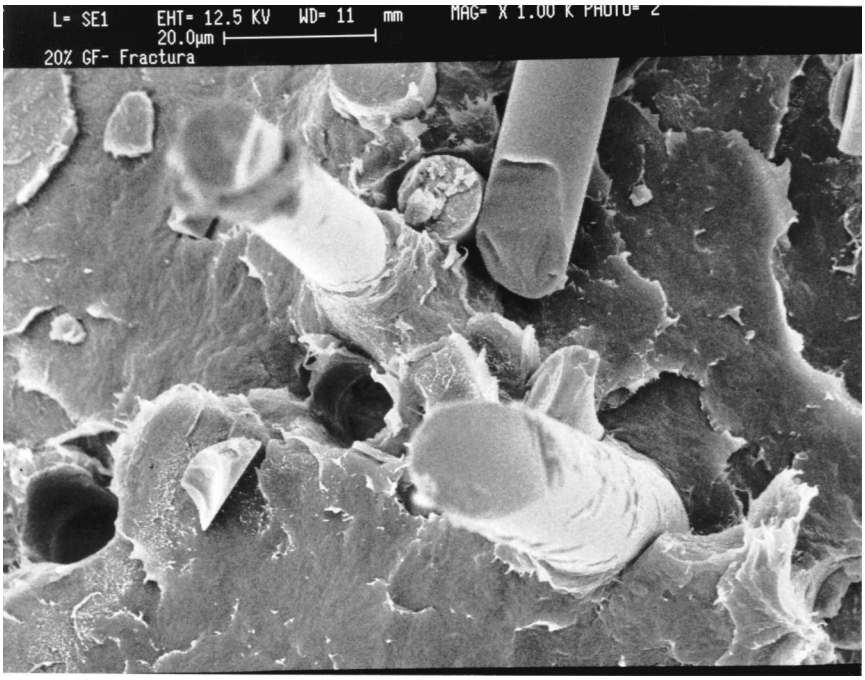

Fig. 7. SEM microphotograph of PP/GF composites after injection molding (1000×).

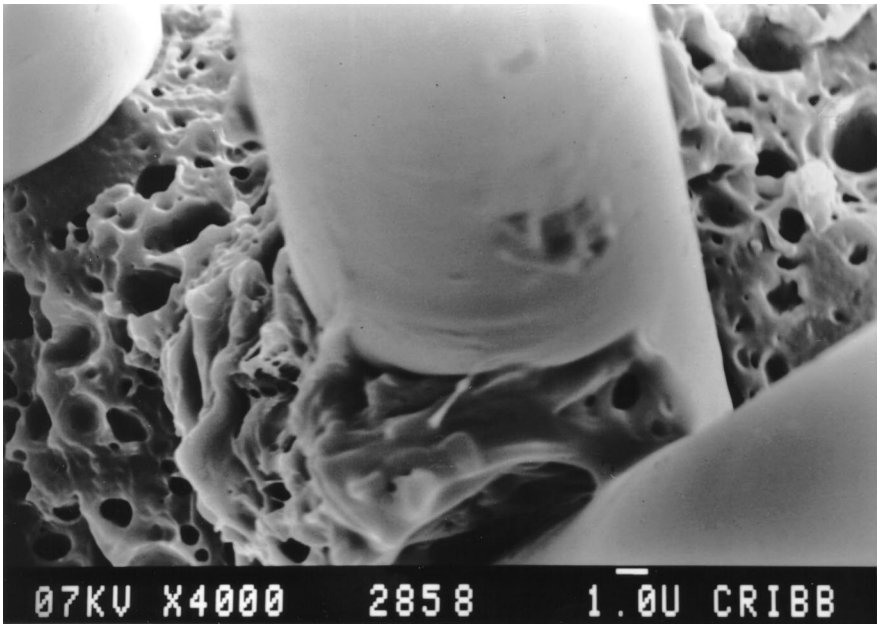

Fig. 8. SEM microphotograph showing fiber-matrix adhesion at high magnification (4000×) in PP/EPDM/GF composites.

4. I. Ward and D. Handley, *Mechanical Properties of Solid Polymers*, J. Wiley (1993).
5. E. Moore Jr., *Polypropylene Handbook*, Hanser Pub. (1996).
6. S. Van der Ven, *Polypropylene and Other Polyolefins*, Elsevier (1990).
7. S. Barbosa and J. Kenny, *J. Reinf. Plast. and Comp.*, 18 **(5)**, 421 (1999).
8. S. Barbosa and J. Kenny, *Polym. Eng. Sci*, (in press) (1999).
9. G. Michler and J. Starke, Chap. 17 in *Toughened Plastics II*, K. Riew and A. Kinloch, eds., ACS (1996).
10. L. A. Utracki, ed., *Two-Phase Polymer Systems*, Hanser Pub. (1991).
11. Y. Yokoyama and T. Ricco, *Polymer*, **39**(16), 3675 (1998).
12. N. Holz, G Goizueta, and N. Capiati, *Polym. Eng. Sci.*, **36**, 2765 (1996).
13. J. Jancar, A. DiAnselmo, A. DiBenedetto, and J. Kucera, *Polymer*, **34**, 1684 (1993).
14. I. Fortelny, E Navratilova, and J. Kovar, *Die Ange. Makrom. Chem.*, **188**(3175), 195 (1991).
15. J. Stamhuis, *Polym. Compos.*, **9**, 72 (1988).
16. F. Stricker and R. Mülhaupt, *Polym. Eng. Sci.*, **38**, 1463 (1998).

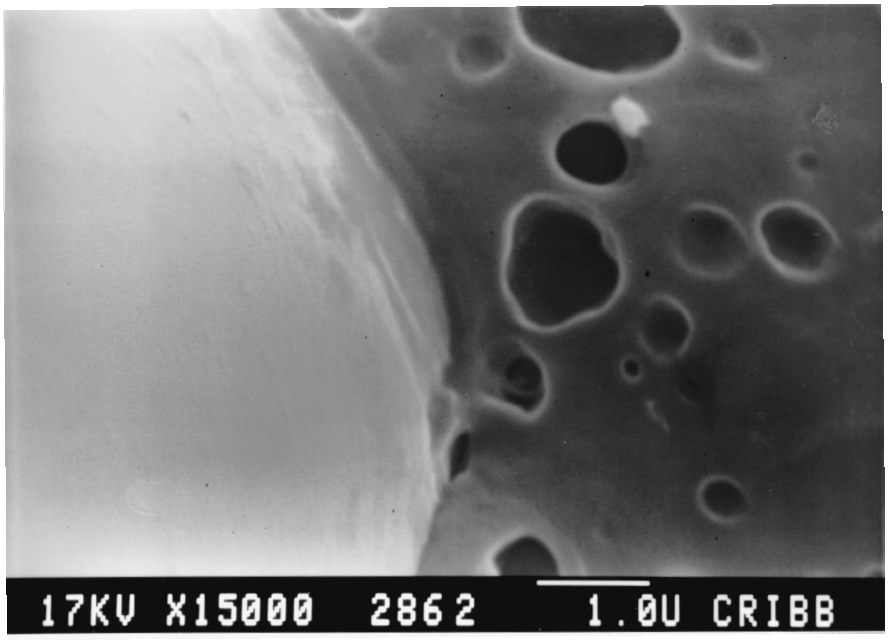

Fig. 9. SEM microphotograph of the fiber/matrix interface at very high magnification (15,000×) in PP/EPDM/GF composites.

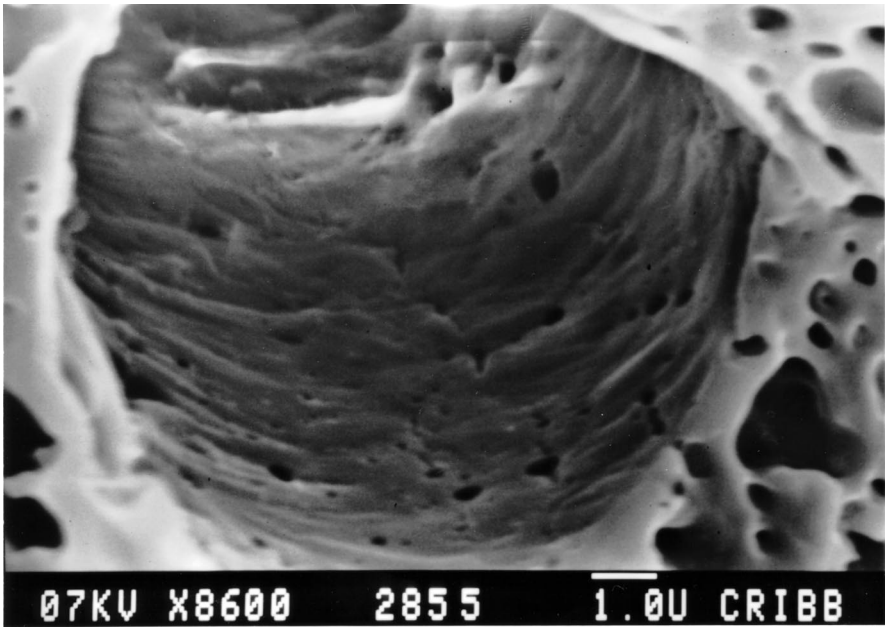

Fig. 10. SEM microphotograph of a "fiber hole" into the matrix in PP/EPDM/GF composites (8600×).

17. C. Scott, H. Ishida, and F. Maurer, *Rheol. Acta*, **27**, 273 (1988).
18. C. Scott and H. Ishida, *J. Mat. Sci.*, **22**, 3963 (1987).
19. M. Dekkeers, J. Dortmans, and D. Hekens, *Polym. Compos.*, **6**, 145 (1985).
20. W. Chiang, W. Yang, and B. Pukánsky, *Polym. Eng. Sci.*, **32**, 641 (1992).
21. F. Stricker and R. Mulhaupt, *J. Appl. Polym. Sci.*, **62**, 1799 (1996).
22. A. K. Gupta, P. K. Kumar, and B. Ratnam, *J. Appl. Polym. Sci*, (42) 2295 (1991).
23. J. Karger-Kocsis, in *Polypropylene, Structure, Blends and Composites*, Vol. 3, p. 142, J. Karger-Kocsis, ed., Chapman and Hall (1995).
24. A. G. Gibson, in *Polypropylene, Structure, Blends and Composites*, Vol. 3, p. 71, J Karger-Kocsis, ed., Chapman and Hall (1995).
25. T. Watanabe and M. Yasuda, *Composites*, 13(54) (1982).
26. A. T. Di Benedetto, *Pure and Appl Chem.*, **57**, 1659 (1985).
27. L. Nicolais, L. Nicodemo, P Masi, and A. Di Benedetto, *Polym. Eng. Sci.*, **19**, 1046 (1979).